Point defects and their reactions in electron-irradiated GaAs investigated by optical absorption spectroscopy

H. Hausmann, A. Pillukat,* and P. Ehrhart
Institut für Festkörperforschung, Forschungszentrum Jülich GmbH, D-52425 Jülich, Germany
(Received 12 February 1996)

Differently doped GaAs crystals were irradiated at 4 K with 0.4- and 2.2-MeV electrons and were investigated by optical absorption spectroscopy with special emphasis on the magnetic circular dichroism of the optical absorption (MCDA). The MCDA yields very characteristic fingerprints of two V_{Ga}-related defects and of the different arsenic antisites As_{Ga}-X_1, As_{Ga}-X_2, and $EL2$. Using these fingerprints the production and the thermally activated reactions of these defects were systematically investigated up to the final annealing at $T_a \approx 850$ K. We show that both sublattices are involved in the defect production even at the lowest electron energies and discuss the importance of replacement collisions. Many antisite defects survive the well-known annealing stages (I to III) of Frenkel pairs. $EL2$ defects seem to be the most stable antisite configuration and are also observed in n-type GaAs that contained no $EL2$ defects before irradiation. A comparison of the spectra obtained after low-temperature irradiations and annealing with spectra obtained after corresponding high-temperature irradiations shows remarkable similarities. All kinds of As_{Ga}-related complexes are usually present simultaneously and we deduce a consistent picture of the visibility of their paramagnetic charge states as a function of doping, irradiation dose, and annealing temperature. [S0163-1829(96)05628-7]

I. INTRODUCTION

Intrinsic point defects in GaAs have been investigated intensively during the last few decades,[1–3] and electron irradiations were widely used to produce defects in the form of Frenkel pairs (FP's) in a reproducible manner. Nevertheless, many basic properties are not yet fully understood. This situation is partly due to the great complexity of the defect pattern in III-V compounds, consisting of different vacancies, interstitial atoms, and antisites, and partly to the fact that the powerful spectroscopic methods are often limited to low defect concentrations and can only detect defects in appropriate charge states; e.g., interstitial atoms seem to be ''invisible'' in many semiconductors. In a preceding paper,[4] we showed by x-ray diffraction (XRD) methods that many of the interstitial atoms are stable in the configuration of close FP's and that rather high concentrations of these FP's can be frozen in at low temperatures. As these methods yield average values for the relaxation volumes over all defects present in the sample we wanted to supplement the results by detailed spectroscopic data on some special defects. These results should be obtained for comparable conditions, i.e., rather high irradiation doses where intrinsic defects are dominant. Optical absorption spectroscopy was chosen as it does not require specially doped samples and it can be applied starting from the irradiation temperature of 4 K. Hence, similar to the XRD investigation, the defect reactions can be investigated from 4 K up to the final annealing at $T_a \approx$ 850 K. The spectral dependence of the magnetic circular dichroism of the optical absorption (MCDA) yields very sensitive fingerprints for defects in charge states characterized by unpaired ''paramagnetic'' electrons. Generally, MCDA spectra involve transitions to several excited states and can at present not be predicted or identified from first-principle calculations. However, this identification may be achieved by optically detected electron paramagnetic resonance (ODEPR) or electron nuclear double resonance (ODENDOR). Especially different As_{Ga}-related complexes have been identified in this way in GaAs.[5] By following these fingerprints after different irradiations we hoped to arrive at a more systematic understanding of the different complexes and of their reactions with other ''invisible'' defects.

Of special interest was a contribution to the long-standing discussion about damage production. By deep level transient spectroscopy (DLTS) a lowest threshold energy for defect production of $T_d \approx 10$ eV (corresponding to a threshold energy for the electron of $E_e = 0.25$ MeV) was determined for GaAs.[1] All the related DLTS signals anneal at a temperature of $T_a \approx 500$ K and were attributed to Frenkel defects on the As sublattice due to the observed dependence of the introduction rate of the defects from the direction of the incident electrons.[1] In spite of the similar atomic masses of As and Ga no defects were observed for these low electron energies on the Ga sublattice and this missing evidence was attributed to the instability (or spontaneous recombination) of the Ga FP's even at the lowest temperatures.[1] For higher electron energies $E_e \geqslant 0.5$ MeV (corresponding to $T_d \approx 20$ eV) additional defects can be produced that anneal between 200 and 330 K; supported by positron annihilation spectroscopy (PAS) these defects are related to vacancies on the Ga sublattice V_{Ga}.[6] This attribution seems to contradict the instability discussed above, however, the high value of T_d indicates that the observed V_{Ga} might be parts of larger defect complexes that are necessary in order to stabilize the Ga FP; double displacements or larger replacement collision chains could yield such stable complexes. In contrast to these earlier conclusions we have recently shown that V_{Ga}-related defects are already produced with 0.4-MeV electrons[7] and in combination with the observation of arsenic antisites[7,8] this shows that both sublattices are involved in the low-energy damage.

0163-1829/96/54(12)/8527(13)/$10.00 © 1996 The American Physical Society

As antisites directly demonstrate the involvement of both sublattices in the damage production we investigated the formation of the different antisite-related complexes in more detail with special emphasis on the comparison of 0.4 MeV and higher energy electron irradiations that permit double displacements.

In Sec. II we give a short description of the experimental methods that are very similar to those of a recent investigation of irradiated InP (Ref. 9) and summarize current knowledge on the fingerprints used below. In Sec. III we present evidence for the different fingerprints as obtained for different irradiation conditions and after different annealing temperatures. In Sec. IV we summarize and discuss the defect production and defect reactions observed during thermal annealing.

II. EXPERIMENTAL METHODS

A. Magnetic circular dichroism of the absorption

The MCDA is defined as the differential absorption of the sample for right (+) and left (−) circularly polarized light that propagates along the direction of the applied magnetic field (see Ref. 10 for review)

$$\mathrm{MCDA} = \frac{d}{4}(\alpha_- - \alpha_+) \tag{1}$$

with $\alpha\pm$ being the respective absorption coefficients and d the thickness of the sample. Within good approximation this quantity can be experimentally determined from the intensities of the transmitted light of polarization ± :

$$\mathrm{MCDA} = \mathrm{const} \times (I^+ - I^-)/(I^+ + I^-). \tag{2}$$

The constant factor is essentially determined by the exact degree of polarization and will be set at 1.0 in the spectra presented below.

Our MCDA spectra were generally taken at 2 K with an applied magnetic field of 5.73 T. The light from a 100-W halogen lamp passed through a 1/4-m double monochromator and was polarized by a combination of a Glan Thomson prism and a photoelastic modulator working at 50 kHz. Without calibration the sign of the MCDA [Eq. (2)] may depend on a phase shift between the modulator and the detection system. Our spectra all have the same absolute signs of the MCDA amplitudes and correspond, e.g., to a positive sign of the maximum at 0.95 eV of the $EL2^+$ in GaAs. A cooled Ge detector was used for photon energies between 0.7 eV and the absorption edge. Using a PbS detector we also monitored the energy range 0.5–0.7 eV for special cases (for details see Ref. 11). For a direct comparison of the different samples all spectra were normalized to correspond to a sample thickness of 100 μm.

During measurements the sample could be illuminated via a mirror from a side entry by a second light source in order to change the population of the defect levels by optical transitions. In this way it is sometimes possible to observe defect states that are not populated in thermal equilibrium for a given position of the Fermi level. As the absolute magnitude of the effects of this ''optical pumping'' is small we will discuss only the changes of the spectra, i.e., the difference of the spectra with and without additional illumination and characterize these spectra by the index p (MCDA_p). The energy of the pumping light was selected by different bandpass filters and the intensity of this light at the position of the sample was $\simeq 15–20$ mW/cm^2.

Using the same light source with a long-pass filter ($\lambda \geqslant$ 850 nm; power at the sample ≈ 200 mW/cm^2) we tested the sensitivity of the defect spectra to optical quenching by illuminating the sample for 10 min at 2 K. This procedure quenches the $EL2$ defects within seconds. In the following we will compare the total MCD spectra as obtained before illumination, MCDA, and spectra obtained after quenching by illumination, MCDA_q. The spectrum of a defect that disappears by quenching as, e.g., $EL2^+$ can be separated from the total background as a ''quenchable'' spectrum: (MCDA-MCDA_q)=MCDA_{qb}. In considering this characteristic feature of a special defect to be quenched (or bleached) by illumination at low temperature it should be kept in mind that this behavior is not unique for defects having a metastable state such as $EL2$, as similar observations may also be caused by mere changes of the charge states. In addition there may be defects that are quenchable under specialized conditions (e.g., high power, single wavelength excitation) but are ''unquenchable'' under our conditions. Hence, a defect such as $\mathrm{As_{Ga}}$-X_1 may be termed ''unquenchable'' under conditions similar to ours,[5] but is termed ''quenchable'' under different conditions by the same authors.[12] In the following changes by quenching always refer to the conditions given above.

B. Fingerprints of different defects

In this investigation we use the MCDA fingerprints of four different $\mathrm{As_{Ga}}$-related complexes that are well documented in the literature, two V_{Ga}-related spectra that have been observed more recently, and a $\mathrm{Ga_{As}}$-related signal. In addition, there is the absorption band of the neutral $EL2^0$ defect and of a band around 1 eV related to an irradiation-induced defect complex.

(i) The $EL2^+$ charge state has a very characteristic MCDA spectrum[5] and this signal can be completely quenched by illumination at low temperatures. In addition there is a diamagnetic MCDA band around 1.19 eV that characterizes the $EL2^0$ charge state.[13]

(ii) A spectrum that is very similar to that of $EL2^+$ but does, however, not show the characteristic optical quenching has been observed after plastic deformation[14] and we will call it $EL2_{\mathrm{pd}}$ for short. The missing quenching has been explained by the presence of additional strain fields[3] and is also observed in ''low-temperature grown'' GaAs layers.

(iii) The $\mathrm{As_{Ga}}$-X_1 defects have only been observed after irradiation. Although the EPR spectrum is not different from the $EL2$ defect, the MCDA is very different. The complex partner X_1 is probably a Ga atom[12,15] and the most recent ODENDOR results[15] suggest a $\mathrm{As_{Ga}}$-$\mathrm{Ga_{As}}$ antisite pair on their respective third-neighbor shells.

(iv) The $\mathrm{As_{Ga}}$-X_2 spectrum is also observed only after irradiation. This MCDA spectrum is obseved only in n-type samples and in spite of some similarities it is easily distinguishable from the $\mathrm{As_{Ga}}$-X_1 spectrum.[5] The EPR spectrum is characterized by a reduced hyperfine interaction as compared to the other $\mathrm{As_{Ga}}$ complexes and has been attrib-

TABLE I. Samples and irradiations.

	Irradiations			Defects characterized by $T_a^{max}(K)^a$ and Σ $(cm^{-1})^{d,f}$ (T/Σ)						
	E_e (MeV)	ϕt (10^{17} cm^{-2})	T_{irr}, T_a^0 [a] (K)	X_{Ga}	V_{Ga}-X	As_{Ga}-X_1	As_{Ga}-X_2	$EL2$[b]	$EL2^+_{pd}$	1-eV band
si1	0.4	60[c]	4/80	80/0.001	–	150/0.002	–			
si2	0.4	131[c]	4/80	80/0.001	–	80/0.001	–			
si3	0.45	36	4/4	80/0.007	–	80/g	–			
si4[e]	2.2	2	4/80	-	80/0.6	330/0.07	–	650/0.02	650/0.02	
si5[e]	2.2	35	4/4	-	80/0.2	330/0.04	–	600.0.04	300/0.12	80/0.30
si6	2.0	52	370/370	-	-	370/0.005	–	370.0.001	370/0.005	
si7	2.0	72	470/470	-	-	470/0.004	–	470/g	470/0.001	470/0.05
si8	2.0	138	670/670	-	–			$670/4\times10^{-5}$	$670/3\times10^{-4}$	-
$n1$	0.4	131	4/80	-	–	330/0.008				
$n2$	2.2	2	4/80	-	[h]	150/g	330/0.1.0			
$n3$	2.2	2.5	4/80	-	80/0.08	360/0.36	500/0.15			
$n4$[e]	2.2	35	4/80	-	80/0.2	500/0.11	-	600/0.05	-	80/0.30
$p1$[i]	0.4	36	4/80							
$p2$[i]	2.2	2	4/80							
$p3$[e]	2.2	35	4/4	330/0.06[j]	80/0.23		–		300/g	330/0.3

[a]T_a^{max} is the annealing temperature where the corresponding signal reaches its maximum amplitude and T_a^0 is the starting temperature of the measurements.
[b]The irradiation induced part of the $EL2^+$ concentration is given for the s.i. samples; $EL2^0$ is given for the n-type sample.
[c]For the 0.4-MeV irradiation the dose is only an estimate that yields an upper limit.
[d]A blank entry indicates that it was not investigated in detail or was not visible due to a low concentration.
[e]Average values for several similar samples.
[f]A hyphen in the entry indicates that the defect is not expected to be visible for these conditions.
[g]Signal identified but no quantitative results due to overlap with other spectra.
[h]Defect visible only with optical pumping.
[i]No visible changes due to the high background signal of the Zn acceptors.
[j]This signal is present also at lower T_a but cannot be determined quantitatively due to overlap with V_{Ga}-X.

uted to a As_{Ga}-V_{As} complex.[8] Other As_{Ga} configurations were proposed later on;[16] however, recent optically detected magnetic resonance (ODMR) investigations[17] strongly support the original model.

(v) After high dose irradiations at low temperatures the MCDA spectrum is dominated by a spectrum with a dominant peak at 0.8 eV.[18] This spectrum has been attributed to a V_{Ga}-related defect.[12,18,19] The asymmetric structure of the MCDA spectrum indicates a low symmetry of the defect that might be attributed to the influence of the interstitial partner of the V_{Ga} within a close Frenkel pair[18] and we will call this defect V_{Ga}-X. ODMR investigations[12] showed that this MCDA correlates with the EPR spectra[20] that were attributed to V_{Ga}^{--}. However, details on possible complex partners and their distances are not yet known.

(vi) A spectrum of similar shape to V_{Ga}-X, but which is shifted by ≈ 0.1 eV to lower energies and which we call X_{Ga} has been observed recently after 0.4-MeV irradiations.[7] From the dependence of this MCDA spectrum on the measuring temperature and on the strength of the magnetic field, we determined a Brillouin function[21] that is compatible with a spin of 1/2 and $g\approx2$ for the ''defect electron.''[7,11] With these values we can correlate this MCDA with an EPR spectrum for a defect with $g=1.99$, $S=1/2$ that has been observed in room-temperature (RT) irradiated p-type GaAs (Ref. 22) and which was attributed to the Ga vacancy in the V_{Ga}^0 charge state.

(vii) Very close to the band edge at $E_{photon}\approx$ 1.45 eV a sharp MCDA line was observed and attributed to Ga_{As} antisite complexes.[23–25] As the transparency of the irradiated samples is very low close to the band edge this line is visible only after annealing at high temperatures in the present experiments and no quantitative results can be deduced.

(viii) Finally, there are two well-characterized absorption bands superimposed on the absorption background. Firstly, the absorption band at 1.1 eV of the $EL2^0$ charge state of $EL2$ (Refs. 3 and 26) and secondly, a band at $\approx$ 1.0 eV with a shoulder at lower energies[27] that is only observed after electron irradiation. This band is remarkably stable up to its annealing temperature of $\approx$ 600 K;[28] however, the microscopic structure of the underlying defect is speculative at present.

C. Samples and irradiations

Samples of sizes 12×6 mm^2 were cut from [100]-oriented wafers of s.i. (undoped), n-type (2×10^{17} Te cm^{-3}) and p-type (2×10^{18} Zn cm^{-3}) liquid-encapsulated Czochralski GaAs and polished to obtain a final

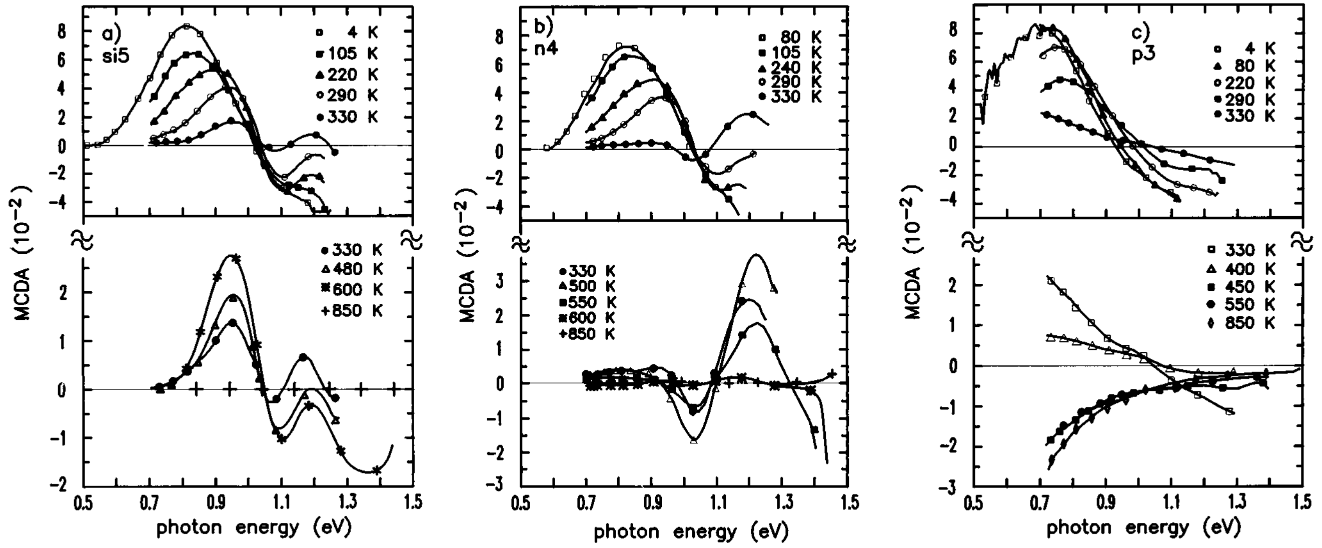

FIG. 1. MCDA spectra as observed after 4-K irradiations (E_e=2.2 MeV, $\phi t=3\times10^{18}e^-/\mathrm{cm}^2$) for s.i. (sample si5) n-type (sample $n4$) and p-type (sample $p3$) GaAs. The spectra at some characteristic annealing temperatures are shown in addition. Within the errors there is complete annealing at 850 K; i.e., the spectra for unirradiated and annealed samples cannot be distinguished.

thickness of 300 μm. These samples were irradiated at 4.5 K with 2.2-MeV electrons in a similar way to the samples for the x-ray investigations.[4] The samples for the 0.4-MeV irradiation had a typical thickness of 130 μm. These samples were rotated by 180° after half of the irradiation dose in order to obtain homogeneous damage. The 0.4-MeV electrons were obtained from a 1-MeV beam that was slowed down by calibrated Cu foils. Therefore there is a broad straggling to lower energies and the electron doses are only approximate and represent an upper limit. The irradiation data are summarized together with the quantitative results in Table I, which is discussed in Sec. III.

After irradiation the samples were transferred into the optical cryostat in liquid helium. The annealing of the samples was performed within an isochronal program with holding times of 15 min. Anneals at temperatures $T_a\leq$RT were performed within the He atmosphere of the cryostat and at higher temperatures within an external furnace under vacuum ($p\leq10^{-4}$ Pa).

III. IRRADIATION-INDUCED FINGERPRINTS

In this section we show examples of the spectra observed after the different irradiations and of the changes observed after the major annealing stages and discuss the production of the underlying defects. An overview of the different irradiations and of the spectra observed is given in Table I. The table contains the annealing temperature at which a certain fingerprint reaches its maximum amplitude in the spectra shown below. As not all measurements were started at T_a=4 K the changes of maximum 15% observed for some spectra at low temperatures are neglected and the values at 80 K are given for a direct comparison. These amplitudes are proportional to the concentrations of the corresponding defects; however, the absolute values of the optical cross sections are not known. For the $EL2^+$ and $EL2^0$ defects absolute concentrations could be deduced from the comparison of the spectra with those of a sample that had been calibrated by EPR.[29] In order to obtain directly comparable values for different samples we included the introduction rate $\Sigma=c/\Omega\phi t$ instead of c in the table (Ω is the atomic volume). For the other defects no calibration is available and we assumed similar cross sections in order to obtain at least an order of magnitude for the concentrations of these defects. Such a procedure is certainly better for the other $\mathrm{As_{Ga}}$-related defects than for the V_{Ga}-related defects. Similar to earlier investigations,[27] we also use the same procedure for the optical absorption by comparing the 1-eV absorption band to the $EL2^0$ absorption band. Although the deduced introduction rates should therefore mainly be considered as a help for the comparison of different irradiations, the values of Σ seem reasonable in the sense that they add up to total values below $\Sigma\approx1\ \mathrm{cm}^{-1}$, which is below the total defect concentration determined by the XRD investigations.[4]

A. MCDA after high dose 2.2-MeV irradiations at 4 K

Figure 1 shows examples of the spectra observed directly after low-temperature irradiation with a dose of $\phi t\approx3\times10^{18}e^-/\mathrm{cm}^2$. For the s.i. sample [Fig. 1(a)] the MCDA is dominated by the V_{Ga}-X spectrum with its peak at $E_{\mathrm{ph}}\approx0.8$ eV. In addition to the standard measurements with the Ge detector that start at $E_{\mathrm{ph}}\approx0.7$ eV the low-energy tail of the spectrum is shown as obtained with a PbS detector. Due to the high defect density the absorption increases very fast close to the band edge and the range of the spectra is limited to $E_{\mathrm{ph}}\leq1.2$ eV at higher energies. After annealing to RT the V_{Ga}-X spectrum disappears and a peak at 1.2 eV that characterizes the $\mathrm{As_{Ga}}$-X_1 defect becomes visible. At $T_a\approx600$ K the $EL2$ spectrum dominates and final annealing is observed for $T_a\approx850$ K. The spectra observed for $T_a<$RT are almost unchanged by optical quenching under conditions that eliminate the as-grown $EL2$ defects completely. The spectra observed for $T_a\geq$RT contain larger quenchable contributions and are discussed below.

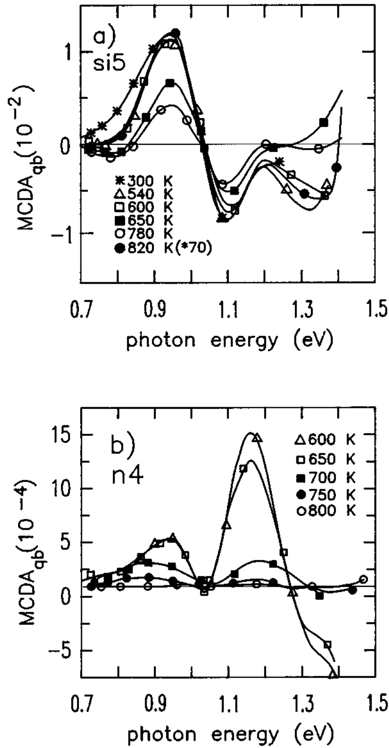

FIG. 2. Quenching behavior of the MCDA after high-temperature annealing of s.i. and n-type GaAs. (a) Quenchable part of the spectra of sample si5. The initial $EL2$ concentration is restored after annealing at 850 K and is lower by a factor of 70 than that observed at 600 K. (b) Quenchable part of the MCDA for the n-type sample $n4$. There is total annealing of the diamagnetic MCDA of the $EL2^0$ defects at 800 K.

The n-type samples [Fig. 1(b)] show similar characteristics; such behavior is expected for high dose irradiations ($c_{\mathrm{FD}} > c_{\mathrm{dop}}$) where the Fermi level is expected close to midgap. During annealing at higher T_a the Fermi level moves back to its initial position and there are corresponding differences of the MCDA spectra from those of the s.i. samples.

The highly doped p-type samples ($c_{\mathrm{FD}} \approx c_{\mathrm{Zn}}$ assuming $\Sigma \approx 1\ \mathrm{cm}^{-1}$) show a similar spectral dependence [Fig. 1(c)]. However, there is an obvious shift of the main peak by 0.1 eV to lower energies. This shift is attributed to the superposition of the X_{Ga} defect that contributes only if the Fermi level is lower than in the s.i. and n-type samples shown in Figs. 1(a) and 1(b). This X_{Ga} spectrum dominates at $T_a \approx 330$ K where most of the V_{Ga}-X defects have annealed and disappears at slightly higher temperatures. This spectrum is visible in more detail for the low-energy irradiations discussed below. For $T_a \geqslant 400$ K the spectra are dominated by the Zn acceptors.

Figure 2 shows some examples of the MCDA observed after annealing at high temperatures in more detail. For the s.i. sample the quenchable part of the MCDA becomes appreciable at $T_a \approx \mathrm{RT}$ and the typical spectrum of $EL2^+$ becomes evident at higher T_a [Fig. 2(a)]. The deduced concentration of $EL2^+$ reaches a maximum at $T_a = 600$ K; as demonstrated by the signal of the annealed sample (850 K), this concentration is higher by a factor of ≈ 70 than in the as-grown state. A very similar signal also remains after quenching; i.e., there must be $EL2$ defects that cannot be optically quenched and we refer to these defects as $EL2_{\mathrm{pd}}$, as discussed above. This signal seems to be already present at lower temperatures (Fig. 1); however, it cannot be identified as clearly due to the limited range of the measurements and to the superposition with the signal of the V_{Ga}-X or $\mathrm{As}_{\mathrm{Ga}}$-$X_1$ defects. Such a superposition of the spectra can also explain the apparent energy shift of the spectra during low-temperature annealing (Fig. 1) in a more consistent way than our initial suggestion of different FP's.[19] Figure 3 shows the modeling of these MCDA spectra by a superposition of the V_{Ga}-X defect with its maximim at 0.8 eV and the $EL2_{\mathrm{pd}}$ defect with its main peak at 0.95 eV if we assume that V_{Ga}-X anneals slowly at low temperatures and $EL2_{\mathrm{pd}}$ is essentially constant. As only the peak at 0.95 eV is visible at low T_a this defect might also be attributed to a spectrum that has been related to the isolated $\mathrm{As}_{\mathrm{Ga}}$;[12] however, as the latter defect has been observed only up to a maximum concentration determined by the initial $EL2$ defects the higher defect concentrations observed here are more reasonably explained by the disturbed $EL2$ defect $EL2_{\mathrm{pd}}$. Irrespective of a possible contribution of the isolated $\mathrm{As}_{\mathrm{Ga}}$, these results show that there are appreciable concentrations of $\mathrm{As}_{\mathrm{Ga}}$-related defects present after irradiation and the quenchable, i.e., undisturbed $EL2$ defects, become dominant only along with the annealing of other defects connected with strong distortion fields.[4]

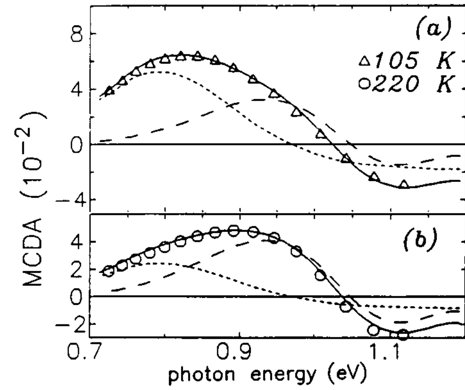

FIG. 3. Example of the fit of the low-temperature MCDA by the superposition of V_{Ga}-X and $EL2_{\mathrm{pd}}$ defects. (a) At $T_a = 105$ K and (b) at $T_a = 220$ K. The shift of the total spectra is due to the decrease of the V_{Ga}-X concentration (sample si5).

Figure 2(b) shows the annealing of n-type GaAs, and we also observe a quenchable spectrum at higher T_a, which by its dominant peak at 1.2 eV can be attributed to the diamagnetic signal of $EL2^0$. The presence of $EL2^0$ is reasonable as at these temperatures E_F starts to move back to the position close to the conduction band. The defect concentrations determined from this MCDA agree quite well with those deduced from the additionally observed absorption band of $EL2^0$. Hence, these results give evidence for the irradiation-induced formation of $EL2$ defects in n-type GaAs not containing $EL2$ defects in the as-grown state.

B. MCDA after low-energy irradiations at 4 K

A completely different spectrum is observed for irradiations with electron energies $E_e < 0.5$ MeV and Fig. 4 shows

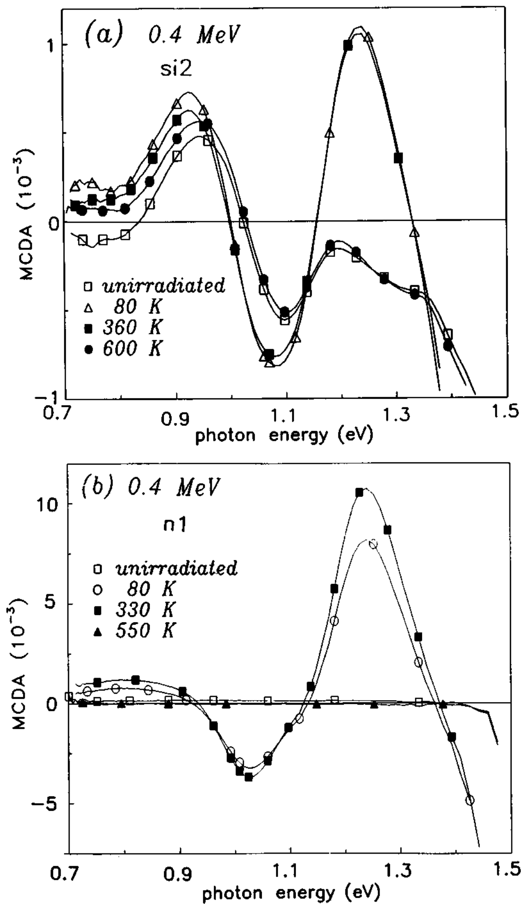

FIG. 4. MCDA spectra of s.i. (sample si2) and n-type (sample $n1$) GaAs after irradiation with 0.4-MeV electrons ($\phi t = 13\times10^{18} e^-/\mathrm{cm}^2$) at 4 K, and after subsequent annealing at different temperatures. The s.i. GaAs is characterized by the superposition of the $EL2^+$ spectrum that is almost unchanged by the irradiation and the As_{Ga}-X_1 spectrum with its peak at 1.25 eV. For the n-type sample only the As_{Ga}-X_1 peak is visible, however, with a much higher amplitude (scale).

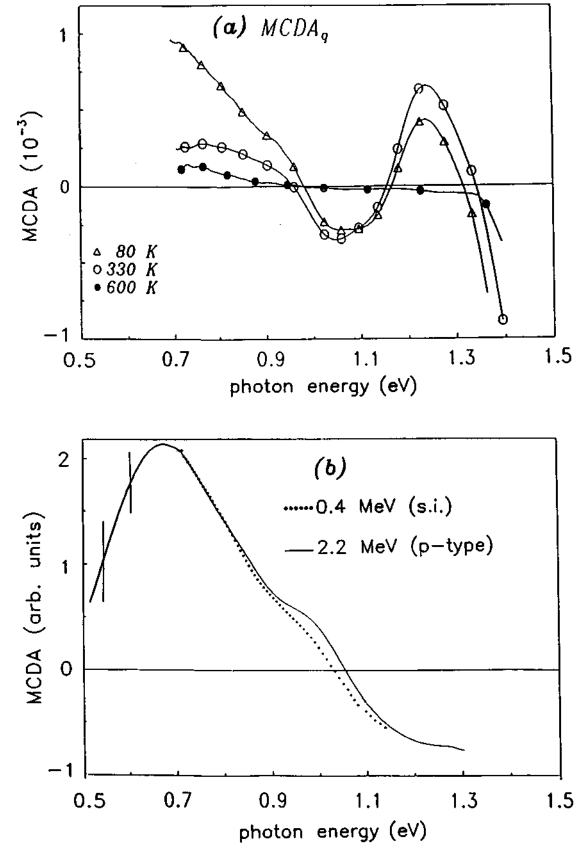

FIG. 5. Evidence for the new X_{Ga} defect from different MCDA spectra: (a) MCDA observed after optical quenching of the s.i. GaAs sample from Fig. 4(a) (0.4-MeV e^- irradiation). (b) Comparison of the spectrum of (a) after subtraction of the As_{Ga}-X_1 contribution to the spectra observed for p-GaAs ($\phi t = 3\times10^{18}$ 2.2 MeV e^-/cm^2) after annealing at 330 K.

the examples of an s.i. and an n-type sample. The s.i. sample is characterized by a superposition of the $EL2^+$-spectrum that is nearly identical to the preirradiated state and the As_{Ga}-X_1 complex with its dominating peak at 1.25 eV. This $EL2$ spectrum is completely optically quenchable with white light at 4 K as it was before irradiation; this behavior is different from higher-energy irradiations where $EL2$ was observed to be destroyed or transformed into another nonquenchable defect, possibly the isolated As_{Ga} (Ref. 5) or $EL2_{pd}$. For n-type GaAs that did not contain $EL2$ defects before irradiation we observe again the formation of As_{Ga}-X_1, however, with a much higher concentration.

Whereas the spectra observed at low annealing temperatures for the high dose irradiations were almost unchanged by optical quenching we observe large changes for the low-energy irradiation [Fig. 5(a)]. As expected the $EL2$ defects have disappeared and the As_{Ga}-X_1, which quenches much more slowly,[12] has decreased; but most prominently we observe a large increase of the amplitude at small photon energies. This increase is markedly different from the V_{Ga}-X spectrum (Fig. 1) and represents the X_{Ga} defect.[7] The related spectrum is shown in Fig. 5(b). The MCDA spectrum of X_{Ga} was obtained from Fig. 5(a) by subtracting the contribution of the As_{Ga}-X_1 defect.

The defect X_{Ga} reaches its MCDA-active paramagnetic charge state only after quenching of $EL2$. As $EL2$ quenches from its neutral charge state $EL2^0$ this quenching yields a decrease of the number of donors and a lowering of the Fermi level and the unirradiated samples become p type. Assuming a similar lowering of the Fermi level in the irradiated samples we can conclude that the X_{Ga} level is located in the lower half of the band gap. This conclusion is supported by the observation that this defect yields a major contribution to the spectra of highly doped p-type GaAs; due to the high MCDA background of the Zn acceptors no significant change could be observed after a low-energy irradiation, but for the higher defect densities of the 2.2-MeV irradiation the X_{Ga} spectrum is present after irradiation and seems to be the dominant defect after annealing at 330 K and this spectrum is included in Fig. 5(b).

With this assumption of an acceptor level for X_{Ga} in the lower part of the band gap the simultaneous observation of X_{Ga} and As_{Ga}-X_1 in the quenched sample [Fig. 5(a)] needs some comment as the latter defect should be in the paramagnetic charge state only for $E_F > E_{VB} + 0.67$ eV.[12] As we have a nonequilibrium population of the carriers after optical quenching at 4 K this level might be partly populated after

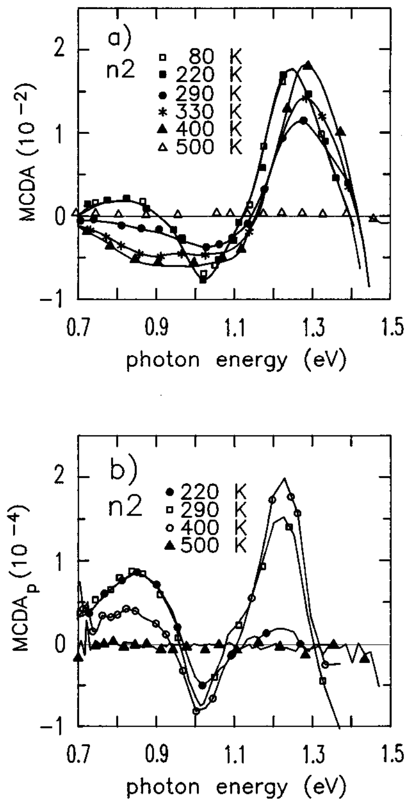

FIG. 6. MCDA spectra observed after low dose irradiation of n-type GaAs and subsequent isochronal annealing at T_a (sample $n2$). (a) Total MCDA; (b) $MCDA_p$ measured under side illumination with a band-pass filter (850 nm).

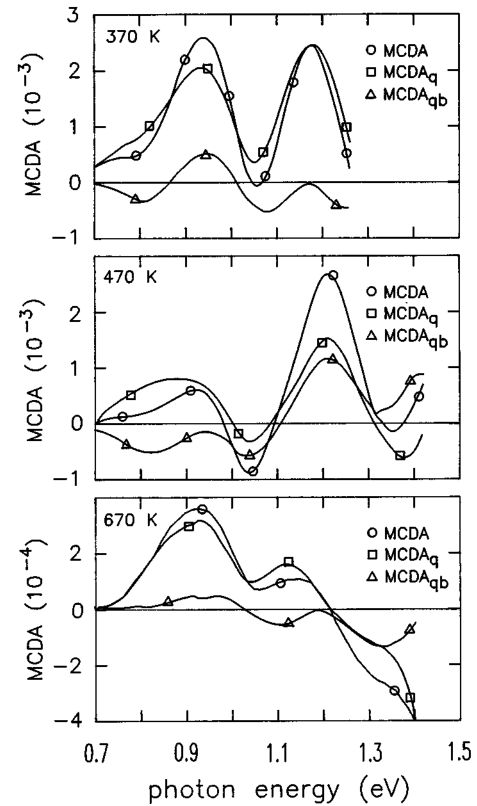

FIG. 7. MCDA spectra observed after irradiations at higher temperatures: (a) 370 K, (b) 470 K, and (c) 670 K. The spectra for irradiation below 500 K contain As_{Ga}-X_1 defects in addition to $EL2$ and $EL2_{pd}$; at higher irradiation temperatures only the $EL2$-related structures can be identified. In addition there is a changing background due to different unidentified defects. The shift of the position of the peak around 1.2 eV between 370 and 470 K is due to a larger contribution of the diamagnetic $EL2^0$ at 370 K. This conclusion is supported by electrical measurements: although all irradiated samples are highly Ohmic ($>10^8$ Ω cm) at RT there is a change from n-type to p-type conduction between these two irradiations.

illumination although the quasi-Fermi level is much lower. This is especially true for the As_{Ga}-X_1 defect, which seems to be a strong electron trap as it shows a similar, although much slower, quenching behavior to $EL2$; hence, the paramagnetic state is a transition state between the equilibrium state for a Fermi level close to the valence band and the ''quenched state'' which might correspond to $(EL2^0)_{\text{quenched}}$. In accordance with these observations, the X_{Ga} defect is not observed in n-type GaAs. Nor is it visible under side illumination; this invisibility under optical pumping does, however, not exclude the presence of the defect in n-type material.

C. MCDA after low dose 2.2-MeV irradiations at 4 K

These low dose irradiations were performed in order to obtain a defect concentration of the As_{Ga}-X_1 defect that is comparable to the 0.4-MeV irradiations. For the s.i. samples the observed results are very similar to the high dose irradiation [Fig. 1(a)]. In contrast to this we observe large changes for the n-type samples [Fig. 6(a)] where the irradiation-induced changes of the Fermi level are important. Similar to the 0.4-MeV irradiation, the As_{Ga}-X_1 concentration is about a factor of 10 higher than for the s.i. samples (Table I). This initially fast increase of the concentration of antisite defects has been observed earlier[30] and seems only to last as long as the samples remain n type; nevertheless it seems to have no relevance for the further defect evolution as there was no relevant difference for the high dose irradiations. Due to this high concentration of As_{Ga}-X_1 the $V_{Ga}-X$ is nearly invisible; however, as Fig. 6(b) shows it is produced and clearly visible under optical side excitation; however, the concentration cannot be determined quantitatively under these conditions.

Figure 6(a) shows in addition a change of the MCDA spectrum during annealing around RT: a shift of the positive peak from 1.25 to 1.28 eV, and a change of the negative amplitude at low photon energies; i.e., we observe the As_{Ga}-X_2 defect instead of the As_{Ga}-X_1 defect for $T_a>$RT. Additional electrical measurements show that the disappearance of As_{Ga}-X_1 and the appearance of As_{Ga}-X_2 is correlated with the movement of the Fermi level back to a position close to the conduction band along with the defect annealing at RT.

D. MCDA after high-temperature irradiations

Figure 7 shows MCDA spectra observed after irradiations at high temperatures of s.i. samples. These spectra can be compared to the spectra obtained after 4 K irradiation and annealing [Figs. 1(a) and 2(a),(b)]. Although there are some

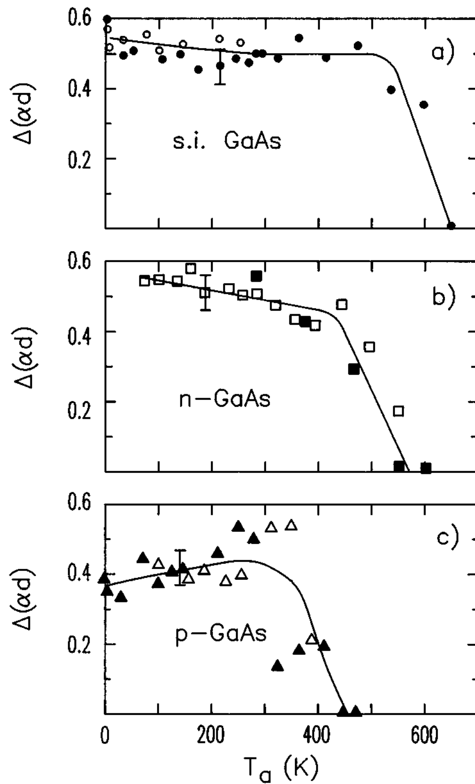

FIG. 8. Annealing behavior of the ''1-eV band'' in s.i., n-type and p-type GaAs after high dose irradiation at 4 K (samples si5, $n4$, $p3$).

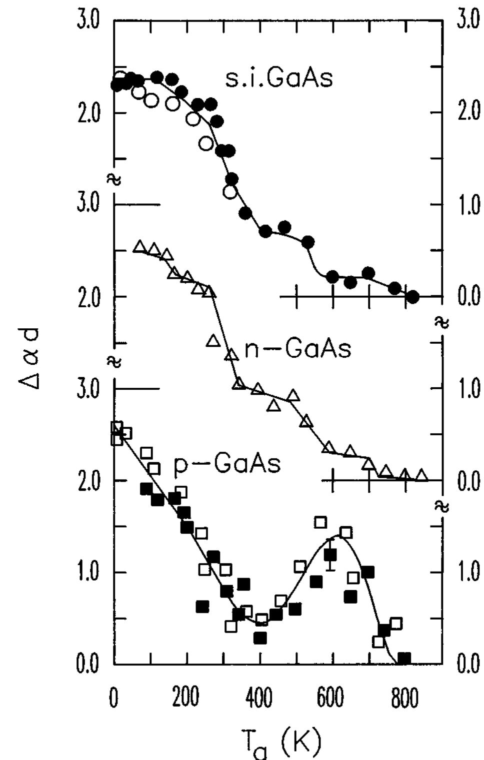

FIG. 9. Annealing behavior of the absorption background at 1.15 eV for high dose irradiations.

differences due to a different background of unidentified defects the dominant defects seem to be very similar. For $T_{irr}=370$ and 470 K we observe As_{Ga}-X_1 as well as $EL2_{pd}$ and smaller amounts of $EL2$ defects. For T_{irr} or $T_a>550$ K the As_{Ga}-X_1 has disappeared and the $EL2$ complexes are the dominating defect species. As can be seen from Table I the introduction rates of these defects decrease with increasing irradiation temperature (however, there are larger uncertainties in the irradiation doses as the irradiations were performed in different irradiation chambers) indicating a higher recombination rate at high temperatures. The spectra remaining after optical quenching indicate in addition the possible presence of some V_{Ga}-X related complexes, in agreement with the incomplete annealing (Fig. 3). The similarity of the defect populations after irradiation and annealing and after high-temperature irradiation indicates that the temporary stabilization of the low-temperature defects is not necessary for the formation of the more stable defects.

Finally, Figs. 7 and 2 show that at temperatures where the accessible range of the spectra exceeds $E_{ph}\approx 1.4$ eV there is a large negative MCDA close to the band edge. This signal remains after optical quenching and reaches its maximum around $T_a=700$ K. The temperature dependence of the MCDA amplitude shows in addition that there is a large paramagnetic MCDA superimposed on a background of diamagnetic origin.[18] The paramagnetic signal indicates the presence of Ga_{As} complexes[23–25] and the diamagnetic part indicates additional acceptors.[23,25] Although we cannot deduce quantitative results these spectra clearly indicate that both types of antisite defects As_{Ga} and Ga_{As} are present up to the final annealing at $T_a\geqslant 800$ K.

E. Optical absorption

The absorption coefficient α is always measured along with the MCDA [Eq. (2)]. For the high dose irradiated samples we observe an irradiation-induced absorption background that increases strongly close to the band edge and the additional absorption band at 1 eV.[27,28]

The ''1-eV band'' consists of a band centered at 0.97 eV and a shoulder at lower energies and has been discussed previously for the s.i. samples.[27,28] The band has a similar intensity for the n-type and p-type samples. However, Fig. 8 shows that the annealing occurs at lower temperatures than for the s.i. samples.

The increase of the background close to the band edge can be understood by the superposition of many different ionization transitions.[32,18] This background increases with the irradiation dose and although this near-band-edge absorption shows no specific features it yields a measure of the total defect concentration. The annealing of the absorption is shown in Fig. 9 for a photon energy of 1.15 eV, where the samples remain sufficiently transparent even after high dose irradiation. For the s.i. and n-type samples we observe a steady decrease with larger stages around RT and between 500 and 600 K. For the heavily doped p-type sample we observe a more complex annealing: a fast decrease for $T\leqslant 400$ K and an increase of α between 400 and 600 K. This annealing behavior is in contrast to the MCDA, which seems to be nearly annealed at $T_a=500$ K as it is dominated by the signal of the Zn acceptors. Hence, the absorption

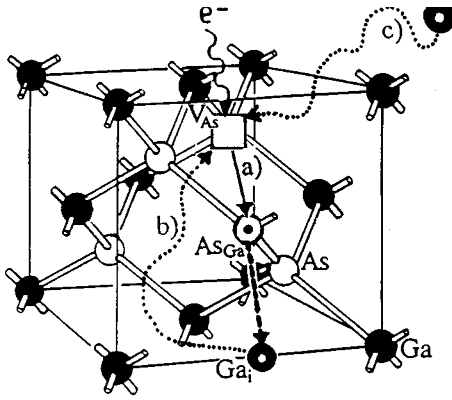

FIG. 10. Schematic view of the production of the As_{Ga}-X_1 defect (As_{Ga}-Ga_{As} antistructure pair on third-neighbor shells) by replacement collisions and mobile interstitials. (a) Replacement collision starting, e.g., at an arsenic atom: $\rightarrow V_{As}+As_{Ga}+Ga_i$. (b) The mobility of the Ga_i may lead to the formation of the antistructure pair; alternatively (not shown) the As_{Ga} may first jump back and complete annealing would arise. (c) The arrival of additional uncorrelated interstitial atoms may lead to the As_{Ga}-X_1 for arriving Ga_i or (not shown) to As_{Ga} that are possibly correlated with Ga_i for the case of arriving additional As_i. If the interstitial already escapes at stage (a) an As_{Ga}-V_{As} complex may arise. The reactions should similarly occur by exchanging the primary knock-on atom with Ga.

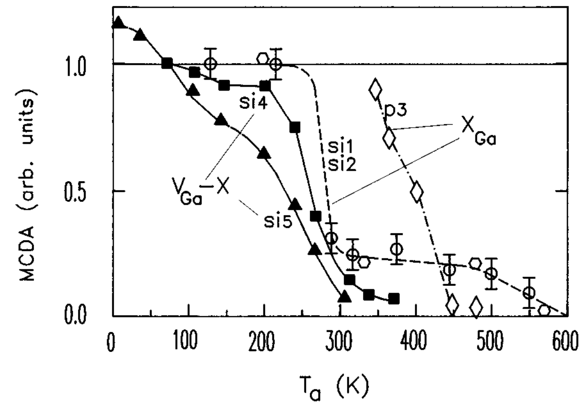

FIG. 11. Annealing behavior of the X_{Ga} defect and the V_{Ga}-X defect as deduced from the MCDA amplitudes at 0.8 eV. Due to the lower concentrations the amplitudes for X_{Ga} have larger error bars. For the p-type sample quantitative results are given only for $T_a > 300$ K due to the initial overlap with the V_{Ga}-X spectrum.

spectra are the only evidence for remaining damage up to a temperature of 850 K where complete annealing is observed for all types of samples. The unique behavior of the p-type samples must be explained by the formation of rather stable Zn-dopand-defect complexes.

IV. DISCUSSION AND CONCLUSION

A. Defect production

The new MCDA spectrum, X_{Ga} (Fig. 5), is observed most clearly after irradiations with 0.4-MeV electrons at 4 K. The spectrum can only be observed if the Fermi level is well below midgap; however, it is shown that the underlying defect is produced and also stable in s.i. samples. Considering all its properties, this defect, X_{Ga}, must be attributed to vacancies on the Ga sublattice.[7] In addition, there might be a correlation to the HNI (hole trap in n GaAs after irradiation) acceptor levels discovered by OMCTS (optical-excitation minority-carrier transient spectroscopy) investigations.[33,34] As these investigations were performed after proton irradiations additional low-energy electron irradiations would be helpful to establish a detailed correlation. Together with the X_{Ga} defect we observe the antisite As_{Ga}-X_1 and these combined observations clearly demonstrate that defects are produced on both sublattices with a threshold energy of $T_d \approx 10$ eV. The threshold energy of ≈ 20 eV must be attributed to complexes resulting from double displacements. Hence, the V_{Ga}-X defect, which shows remarkable similarities to X_{Ga}, should be part of such complexes. The formation of complexes also directly explains the large relaxation volumes of $V^{rel} \approx 2\ \Omega$ or the corresponding large displacement fields connected with these defects.[4] With this attribution the atomic relaxations around single intersititials and vacancies in GaAs are very similar to those of other semiconductors such InP,[35,36] Ge,[31,37] and Si.[37]

As the atomic structure of these defects, which is essentially based on ENDOR results, is a matter of some controversy especially for the $EL2$ defect,[2,3] we have so far presented conclusions that are independent of the details of the models. However, if we consider, e.g., the recent attribution of the As_{Ga}-X_1 defect to a As_{Ga}-Ga_{As} complex[15] very detailed models of the damage process can be deduced. As indicated in Fig. 10, the combination of replacement collisions and at least a short-range interstitial mobility is necessary to produce this defect by 0.4-MeV electrons at 4 K. In addition, it is conceivable that one of these steps leading to As_{Ga}-X_1 or As_{Ga}-X_2 might be strongly favored as long as the GaAs is n type and hence explains the large initial introduction rate discussed above and the final decrease of Σ if the Fermi level is lowered. Irrespective of the model, our data show that As_{Ga}-X_1 cannot be considered as a product of reactions of precursor defects at RT as suggested by the high-energy irradiations.[15]

Finally, the very similar defect spectra observed after low-temperature irradiation and annealing as compared to high-temperature irradiations show that the defect production mechanisms are very similar for both cases. However, the number of surviving defects decreases with temperature. As seen by XRD,[4,31] this decreasing number of point defects must be due to recombination of FP's and not to the formation of large defect clusters such as dislocation loops.

B. Thermally activated defect reactions

In this section we discuss the different defect types, V_{Ga}-related defects, As_{Ga} defects, and the ''1-eV band,'' separately and finally compare the annealing of the spectroscopic fingerprints with the annealing of the total defect population. For ease of comparison some annealing curves are normalized and we refer to Table I for a comparison of the concentrations.

1. V_{Ga}-related defects

The annealing of the V_{Ga}-related defects is shown in Fig. 11. Most of the X_{Ga} defects anneal around RT; i.e., these spectra are the first indication of a defect produced with $E_e \leq 0.5$ MeV that anneals below 500 K. The annealing in p-type material seems to be delayed by ≈ 100 K and due to

this delayed annealing it seems plausible that the same defect was observed by EPR after RT irradiation.[22] The annealing of X_{Ga} is very similar to the annealing of V_{Ga}-X; however, the V_{Ga}-X defects anneal around 300 K independent of the doping. In spite of the uncertainties due to superpositions with other defect spectra, we observe a survival of 10%–20% of the V_{Ga} defects at 330 K. Such a residue is expected if the V_{Ga} defects anneal by recombination with mobile interstitial atoms as some interstitials find other deep traps and do not find a vacancy; this conclusion is supported by EPR results[38] that yield evidence for V_{Ga} defects up to much higher temperatures.

We conclude that the annealing of V_{Ga} defects is a dominant defect reaction within the range of Thommens annealing stages I and II (200–350 K).[39] This conclusion is in agreement with PAS results[6] although a defect has not yet been found which corresponds to X_{Ga}. The reactions observed for the As_{Ga}-related defects discussed below show, in addition, that the defect reactions are not simply restricted to the Ga sublattice.

2. As_{Ga}-related defects

Figure 12 summarizes the annealing of the As_{Ga}-antisite defects observed after different irradiations. Figures 12(a) and 12(b) show the different behavior of As_{Ga}-X_1 in s.i. and n-type GaAs as observed after 0.4- and 2.2-MeV irradiation. As_{Ga}-X_1 is the dominating defect after 0.4-MeV irradiation; however, for the higher energy irradiations the As_{Ga}-X_1 defect is no longer observed at low temperatures; it remains undetectable even under side illumination during the measurement. In agreement with earlier investigations[12,19] the defect appears, however, after annealing through the RT-annealing stage. Irrespective of these differences, final annealing of As_{Ga}-X_1 is observed around 600 K. The annealing is even more complex in n-type GaAs, as shown in Fig. 12(b). We observe As_{Ga}-X_1 immediately after 0.4 MeV and also after low dose 2.2-MeV irradiation. However, in this case the defect already disappears at RT. With increasing dose we observe the same behavior as in s.i. GaAs.

The As_{Ga}-X_2 defect [Fig. 12(c)] shows a remarkable anticorrelation to A_{Ga}-X_1: if As_{Ga}-X_1 already disappears at $T_a \leq 550$ K the As_{Ga}-X_2 appears and finally also anneals around 550 K. A corresponding change of the visibility has been observed by EPR after RT irradiations as a function of the irradiation dose:[8] at very low doses the signal now attributed to As_{Ga}-X_2 was observed and another As_{Ga}-related defect appeared along with the shift of the Fermi level at doses corresponding to our lowest dose. Starting from this observation a transformation of the two defects by defect reactions during prolonged irradiation has been speculated (i.e., As_{Ga}-V_{As}+$As_i \rightarrow As_{Ga}$).[8] However, the present observation of a back-transformation during annealing at different temperatures excludes such processes. As suggested by theoretical calculations,[40] the disappearance of the As_{Ga}-X_2 defects has also been correlated with a Fermi-level-dependent instability of the Ga vacancy: $V_{Ga} \rightleftharpoons As_{Ga}$-$V_{As}$.[41] This correlation seems, however, very problematic as the experimental observations would yield a dependence of the stable configuration on the position of the Fermi level that is opposite to the calculation. In addition, the anticorrelation with As_{Ga}-X_1 is not explained.

In order to check for a simple Fermi level (or charge state) dependence of the visibility of the two different As_{Ga}-X defects measurements were repeated under optical side excitation and indeed the two defects were observed simultaneously under these conditions. However, this simultaneous visibility is limited to annealing temperatures close to the change of the visibility, i.e., 250–350 K for sample $n2$ and 400–550 K for sample $n3$. The failure of the optically induced recharging far off this region may be due to different reasons and does not exclude the presence of the defect in a ''wrong'' charge state. Combining all observations we conclude that both defects are simultaneously present and that the changes of the visibility of the two defects must be understood as a function of the shift of the Fermi level as summarized in Fig. 13.

Figure 12(d) summarizes the reactions of the $EL2$ defect as they are deduced for s.i. samples from the amplitude of the main peak at 0.95 eV. After irradiation there hardly any ''quenchable'' $EL2$ defects are observable. However, a nonquenchable $EL2_{pd}$ spectrum can be observed (Fig. 3) in spite of the superimposed V_{Ga}-X spectrum; along with the RT annealing the number of these defects decreases and quenchable defects can be detected. This behavior can be understood within the model[3] developed for the defects in plastically deformed GaAs if these $EL2$ defects are located close to the strongly distorting Frenkel defect complexes[4] that anneal around RT. During further annealing these quenchable $EL2$ defects increase in number and reach around 600 K a maximum concentration that is much higher than in the unirradiated samples. In n-type GaAs the Fermi level rose during annealing and at 600 K there is the first clear evidence for the presence of $EL2^0$ defects in irradiated n-type GaAs from the diamagnetic MCDA band[13] observed first in s.i. GaAs. Remarkably, the final increase of the $EL2$ concentration coincides with the disappearance of the As_{Ga}-X defects and in this case indicates a transformation of the configuration of the As_{Ga} complexes. In addition it is remarkable that $EL2$ is formed here in n-type GaAs, where no $EL2$ is formed by thermal treatment.[3] The final annealing of these most stable complexes is observed between 800 and 850 K and, independent of the presence of $EL2$ in the starting wafers, the initial concentration is obtained again (i.e., $EL2^+ + EL2^0 \approx 2 \times 10^{16}$ cm^{-3} for s.i. and ≈ 0 for n-type GaAs). As the native $EL2$ defects are stable up to much higher temperatures[2,3] this annealing cannot be attributed to a thermal decay of an $EL2$ complex; it rather means that the radiation-induced $EL2$ defects anneal by reactions with other mobile defects and this must be the vacancies that can be assumed to be mobile in this temperature region.[2] Due to the similarity of the EPR spectra of As_{Ga}-X_1 and $EL2$ on the one hand and the different optical quenching behavior of these defects ($EL2$ fast, As_{Ga}-X_1 very slow, $EL2_{pd}$ unquenchable) there has been some controversy about the behavior of the As_{Ga}-related defects[42] and only by the additional use of the MCDA could we obtain a clear discrimination.

Figure 13 finally summarizes the visibility ranges of the different As_{Ga} complexes and V_{Ga} complexes along with the shift of the Fermi level during irradiation and its moving back during thermal annealing, as has been discussed with the data from Fig. 12. There is only limited information for our heavily doped p-type GaAs as the Zn acceptors dominate

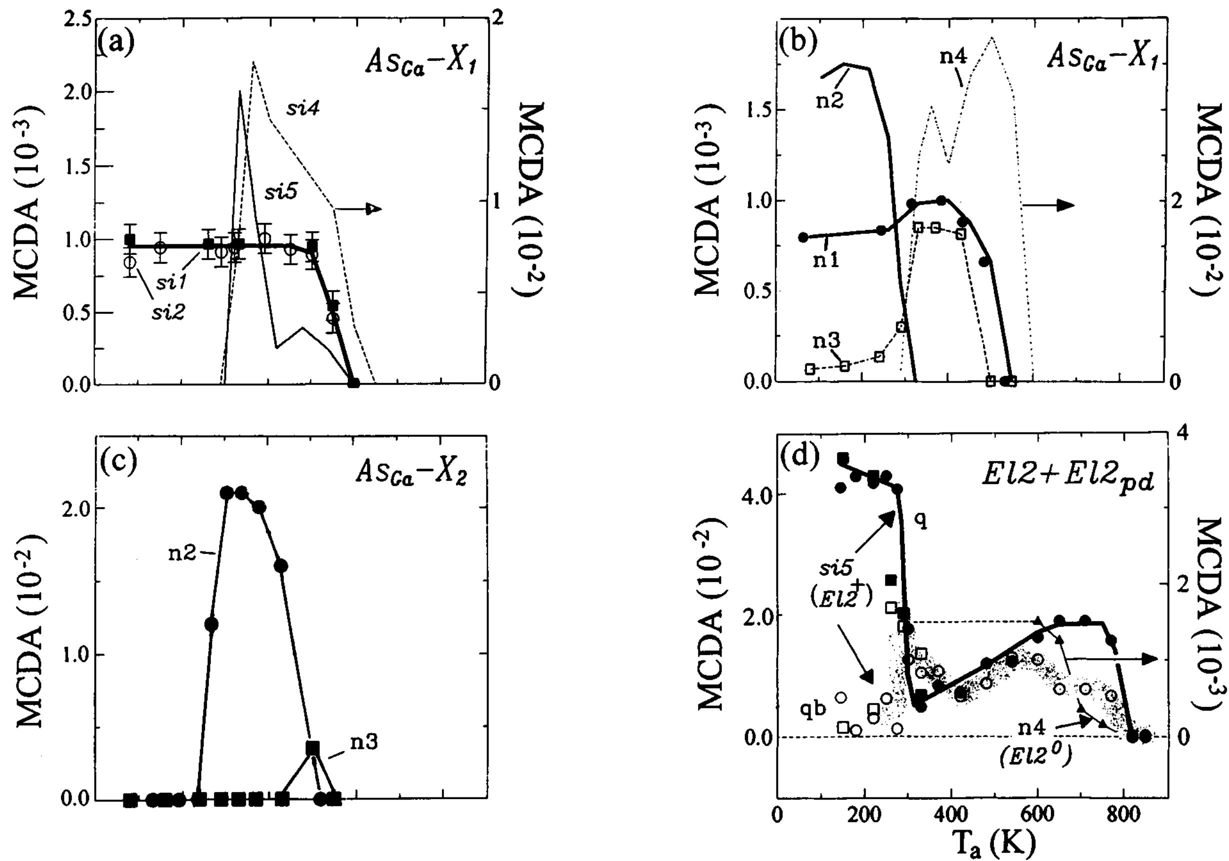

FIG. 12. Build-up and decay of different As_{Ga}-related MCDA spectra during irradiation and subsequent isochronal thermal annealing at temperatures T_a. (a) As_{Ga}-X_1 in s.i. GaAs: after 0.4-MeV irradiation (si1, si2) the spectrum is directly observed after 4-K irradiation whereas after 2.2-MeV irradiation the spectrum is only observed after annealing around RT; the details of the annealing depend on the irradiation dose (si4, si5). (b) As_{Ga}-X_1 in n-type GaAs: after 0.4-MeV irradiation (n1) the spectrum is observed at 4 K and anneals around 550 K; after 2.2-MeV irradiations ($n2$, $n3$, $n4$) there is a dose dependence of the visibility. (c) As_{Ga}-X_2 in n-type GaAs: the figure shows the anticorrelation to Fig. 1(b), i.e., if X_1 disappears at $T_a<550$ K X_2 becomes visible. (d) $EL2^+$ and $EL2^+_{pd}$ in s.i. GaAs after high dose irradiations (si5); data below 550 K have larger uncertainties because of the overlap with other spectra; the as-grown $EL2^+$ concentration ($\approx 5\times10^{15}\ \mathrm{cm}^{-3}$) is reached at 800 K and is nearly invisible on this scale. In addition the annealing of $EL2^0$ in n-type GaAs (n4) is shown as determined from the diamagnetic MCDA line and from the optical absorption band at 1.18 eV.

the MCDA after low-energy and low dose irradiations. Only after higher dose irradiations are the V_{Ga} signals observed. After annealing to RT there is some indication of $EL2_{pd}$; at higher annealing temperatures the Zn acceptors again dominate the MCDA although the optical absorption again indicates the presence of radiation defects up to 800 K.

3. The 1-eV absorption band

The annealing of the 1-eV band is summarized in Fig. 8; this band is thermally very stable in s.i. GaAs as discussed earlier.[28] For the n-type GaAs there is small and steady annealing up to 450 K and faster annealing up to 600 K. For p-type GaAs there are larger errors due to the larger variations of the background and final annealing is observed at 450 K. Independent of the doping, there is no indication that the signal is dependent on the position of the Fermi level as it cannot be changed by quenching or optical pumping. Hence, this band is correlated with a very stable defect that is not correlated with any of the MCDA fingerprints and does not react with the defects mobile in stages I and II. This stability might be explained by a Coulomb repulsion of these mobile defects and the faster annealing in p-type material can therefore be explained by a different charge state of a defect mobile around 400 K in p-type GaAs. We might speculate about mobile Zn_i formed by a kick-out mechanism which react with these defects and also cause the increased absorption at higher photon energies (Fig. 9).

4. Comparison to averaging signals

Figure 14 summarizes the annealing of the optical absorption background close to the band edge, i.e., at 1.15 eV for the high dose irradiations and compares this signal to the annealing of the change of the lattice parameter and of the diffuse scattering intensity.[4] Although the highest dose of the present investigation is at the lowest end of the XRD investigations, these data can be directly compared as both results are essentially linear in dose. All these quantities represent—differently weighted—average signals over all defects, and these curves might therefore be used as an indication of the behavior of the total defect concentration. In addition to the

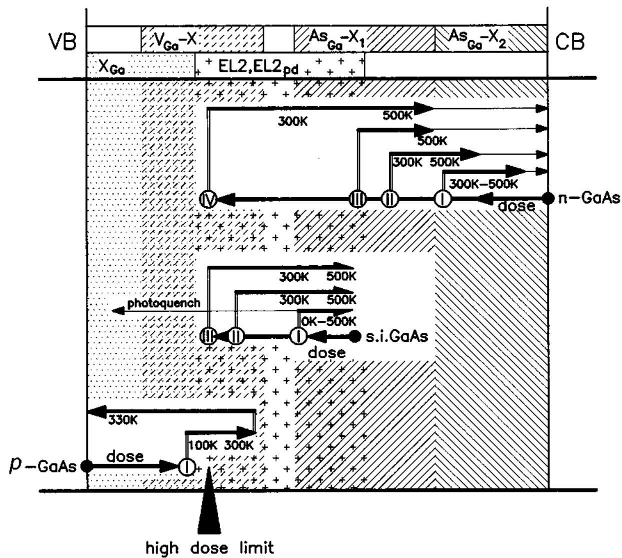

FIG. 13. Schematics of the dependence of the visibility of the paramagnetic MCDA spectra of different As_{Ga}-related complexes and of the V_{Ga}-related defects V_{Ga}-X and X_{Ga} as a function of the position of the Fermi level. The valence band is indicated at the left-hand side and the conduction band at the right-hand side. The ranges of the paramagnetic charge states of the defects, which partly overlap, are indicated by different hatching of the background. Starting from the Fermi level of the differently doped samples (s.i., n-, p-type) the arrow ''dose'' indicates the movement of the Fermi level to the limiting position after high dose irradiation ($\approx E_{VB}+0.5$ eV). The numbers indicate the starting point of different annealing programs after increasing irradiation doses and the temperatures indicate the annealing temperature at which this level might be reached. Regions that may be crossed at temperatures where the corresponding defects have already annealed are indicated by thinner arrows. The annealing point 1 for the n-type GaAs is deduced from Ref. 6.

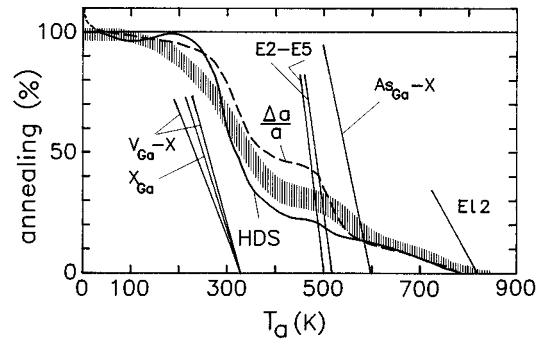

FIG. 14. Annealing behavior of the near-band-edge optical absorption in s.i. and n-type GaAs. The area of the hatched annealing curve includes the variations between the different samples. There is remarkable similarity to the annealing behavior of the Huang diffuse scattering and of the change of the lattice parameters (Ref. 4) and all these data reflect the total defect concentration. The annealing behavior of some optically detected fingerprints and of the most prominent DLTS levels (E_2-E_5) (Ref. 43) is shown for comparison.

dominant annealing stages (I and II) around room temperature and the annealing stage III at $T_a \approx 500$ K (Ref. 1) we observe more or less steady annealing starting at the lowest temperatures. The annealing of the fingerprints discussed above is included schematically together with the most prominent DLTS levels $(E2-E5)$.[43]

Together with the introduction rates summarized in Table I the relative importance of the different fingerprints to the total defect spectrum can be seen from the comparison of the defect annealing. We conclude that most fingerprints must represent minority defects out of the broad defect spectrum present after high dose irradiations, which add up to the introduction rate of $\Sigma > 2$ cm^{-1} deduced from XRD.[4] Considering the high annealing background the different rather independent defect reactions of some fingerprints indicate rather local defect rearrangements and the influence of Coulomb repulsion of charged mobile defects at low temperatures. Nevertheless, we now have fingerprint reactions over a wide range of T_a and the broad distribution of the different defect types reveals some trends. The low-temperature annealing stages I,II are characterized by the annealing of the V_{Ga}-related defects V_{Ga}-X and X_{Ga}. From the large value for the average displacement field around these defects[4] we conclude that the x-ray results are dominated by closely correlated defects resulting from double displacements and that these defects can be related to the V_{Ga}-X spectrum due to the high threshold energy. Stage III was originally assigned to the sharp stage of the DLTS levels at 500 K; however, the results of Fig. 14 indicate that a larger number of defects anneal within a range up to $T_a \approx 600$ K, i.e., this annealing stage starts with the annealing of close As FP's (Refs. 1 and 43) and ends with the final disappearance of the special As_{Ga} complexes (-X_1 and -X_2) and the 1-eV band only observed after irradiation. These latter reactions indicate the beginning of vacancy migration at this temperature. The As_{Ga} complexes $EL2$ and $EL2_{pd}$ are additionally produced in large numbers by the irradiation and can be transformed into their special structure due to interaction with other defects. These $EL2$ defects are the most stable complexes as their final annealing is observed within the region between 600 and 850 K along with the increasing mobility of vacancies on both sublattices and the possible dissolution of small vacancy complexes. After this stage the original defect equilibrium is reached again as we obtain the preexisting $EL2$ concentration in s.i. samples and have no $EL2$ defects left in n-type samples that originally contained no $EL2$ defects. As a final comment we would like to recall the remarkable similarities to the defect reactions observed with InP.[9]

ACKNOWLEDGMENTS

We would like to thank Professor W. Schilling for his continuous support for this work and many helpful discussions. We gratefully acknowledge the technical assistance of W. Bergs and the support from Dr. F. Dworschak and J. Fink in the course of the electron irradiations and we thank M. Kloke for high-temperature irradiations. Last but not least we are grateful for the support from Professor J.-M. Spaeth and his co-workers Dr. Lohse and Dr. Krambrock at the beginning of these investigations.

*Present address: Jena Optronic GmbH, Prüssingstrasse 41, 07745 Jena, Germany.

[1] D. Pons and J.C. Bourgoin, J. Phys. C **18**, 3839 (1985).
[2] J.C. Bourgoin, H.J. v. Bardeleben, and D. Stiévenard, J. Appl. Phys. **64**, R65 (1988).
[3] M. Kaminska and E.R. Weber, in *Imperfections in III/V Materials*, edited by E.R. Weber, Semiconductors and Semimetals Vol. 38 (Academic, New York, 1993), p. 59.
[4] A. Pillukat, K. Karsten, and P. Ehrhart, Phys. Rev. B **53**, 7823 (1996).
[5] J.-M. Spaeth, M. Fockele, and K. Krambrock, Mater. Sci. Eng. B **13**, 261 (1992).
[6] C. Corbel, F. Pierre, P. Hautojärvi, K. Saarinen, and P. Moser, Phys. Rev. B **41**, 10 632 (1990).
[7] H. Hausmann and P. Ehrhart, Mat. Sci. Forum **196/201**, 1255 (1995).
[8] H.J. v. Bardeleben, A. Miret, H. Lim, and J.C. Bourgoin, J. Phys. C **20**, 1353 (1987).
[9] H. Hausmann and P. Ehrhart, Phys. Rev. B **51**, 17 542 (1995).
[10] P.J. Stephens, in *Advances in Chemical Physics* Vol. 35, edited by I. Prigogine and S.A. Rice (Wiley, New York, 1976), p. 197.
[11] H. Hausmann, Report KFA Jülich No. JÜL-3005/1994 (unpublished).
[12] K. Krambrock and J.-M. Spaeth, Mater. Sci. Forum **83/87**, 887 (1992).
[13] A. Pillukat and P. Ehrhart, Appl. Phys. Lett. **60**, 2794 (1992).
[14] D.M. Hofmann, B.K. Meyer, J.-M. Spaeth, M. Wattenbach, J. Krüger, C. Kiesilowski-Kemmerich, and H. Alexander, J. Appl. Phys. **68**, 3381 (1990).
[15] K. Krambrock and J.-M. Spaeth, Phys. Rev. B **47**, 3987 (1993).
[16] H.J. v. Bardeleben, C. Delerue, and D. Stiévenard, Mater. Sci. Forum **143/147**, 223 (1994).
[17] K.H. Wietzke, F.K. Koschnick, and J.-M. Spaeth, Mater. Sci. Forum **196/201**, 1061 (1995).
[18] A. Pillukat, Report KFA Jülich No. JÜL-2547, 1991 (unpublished).
[19] A. Pillukat and P. Ehrhart, Mater. Sci. Forum **83/87**, 947 (1992).
[20] Y.Q. Jia, H.J. v. Bardeleben, D. Stiévenard, and C. Delerue, Phys. Rev. B **45**, 1685 (1992).
[21] A. Görger, B.K. Meyer, J.-M. Spaeth, and A. Hennel, Semicond. Sci. Technol. **3**, 832 (1988).
[22] Y.Q. Jia and H.J. v. Bardeleben, Phys. Lett. A **178**, 205 (1993).
[23] B.K. Meyer, Mater. Sci. Forum **38/41**, 59 (1989).
[24] K. Krambrock, B.K. Meyer, and J.-M. Spaeth, Phys. Rev. B **39**, 1973 (1989).
[25] K. Krambrock, B.K. Meyer, and J.-M. Spaeth, in *Proceedings of the 5th International Conference on Semiinsulating III-V Materials*, edited by G. Grossman and L. Ledebo (IOP, London, 1988), p. 159.
[26] M. Kaminska, M. Skowronski, J. Lagowski, J.M. Parsey, and H.C. Gatos, Appl. Phys. Lett. **43**, 302 (1983).
[27] M.O. Manasreh and D.W. Fischer, Appl. Phys. Lett. **53**, 2429 (1988).
[28] A. Pillukat and P. Ehrhart, Phys. Rev. B **45**, 8815 (1992).
[29] K. Krambrock (private communication).
[30] R.B. Beall, R.C. Newman, J.E. Whitehouse, and J. Woodhead, J. Phys. C. **18**, 3273 (1985).
[31] P. Ehrhart, K. Karsten, and A. Pillukat, in *Beam-Solid Interactions: Fundamentals and Applications*, edited by M. Nastasi, L.R. Harriott, N. Herbots, and R.S. Averback, MRS Symposia Proceedings No. 279 (Materials Research Society, Pittsburgh, 1993), p. 75.
[32] A. Chantre, G. Vincent, and D. Bois, Phys. Rev. B **23**, 5335 (1981).
[33] W.O. Siyanbola and D.W. Palmer, Phys. Rev. Lett. **60**, 56 (1991).
[34] A.C. Irvine and D.W. Palmer, Phys. Rev. B **49**, 5695 (1994).
[35] K. Karsten and P. Ehrhart, Mater. Sci. Forum **143/147**, 365 (1994).
[36] K. Karsten and P. Ehrhart, Phys. Rev. B **51**, 10 509 (1995).
[37] S. Bausch, H. Zillgen, and P. Ehrhart, Mater. Sci. Forum **196/201**, 1141 (1995).
[38] A. Goltzené, B. Meyer, and C. Schwab, J. Appl. Phys. **57**, 1332 (1985).
[39] K. Thommen, Radiat. Eff. **2**, 201 (1970).
[40] G.A. Baraff and M. Schlüter, Phys. Rev. Lett. **55**, 2340 (1985).
[41] H.J. v. Bardeleben, J.C. Bourgoin, and A. Miret, Mater. Sci. Forum **10/12**, 299 (1986).
[42] M.O. Manasreh, D.W. Fischer, and W.C. Mitchell, Phys. Status Solidi B **154**, 11 (1989).
[43] D. Pons, A. Mircea, and J.C. Bourgoin, J. Appl. Phys. **51**, 4150 (1980).